Distyrylbenzene-based segmented conjugated polymers: Synthesis, thin film morphology and chemosensing of hydrophobic and hydrophilic nitroaromatics in aqueous media

Marcela F. Almassio,[‡] Maria J. Romagnoli,[‡] Pablo G. Del Rosso, Ana Belén Schwal and Raúl O. Garay*

INQUISUR, Departamento de Química, CONICET, Universidad Nacional del Sur, Alem 1253, CP 8000 Bahía Blanca, Argentina

***Corresponding author**: Prof. Raúl O. Garay. Tel.: +54 291 4595101; fax: +54 291 4595187. E-mail address: rgaray@criba.edu.ar

[‡]Both authors contributed equally to this work

Abstract

Two new segmented conjugated polymers bearing distyrylbenzene chromophoric units and their model compounds were synthesized. The tendency of the model compounds to form H- and J-type aggregates in the amorphous matrix was greatly diminished by the twisted polymeric architecture. Fluorescence anisotropy measurements indicated good exciton mobilities in condensed phase. Fluorescence quenching by nitroaromatic aqueous solutions was fast, complete, selective and reversible pointing to a rapid diffusion of analytes into the films. The quenching response to nitrophenols was superior to that against nitrotoluenes. The increase of the electron-donating capabilities by diethoxy-substitution was detrimental to the amorphous morphology and it did not increase sensitivity to NACs. Quenching efficiencies of polymers were not modified when MeOH was used instead of water. The solubility parameter distances, R_a, indicate that the sensing materials show higher responses when their affinity with the analytes is lower. This observation could help in the designing of fluorescent sensors.

Keywords
Segmented conjugated polymer
Fluorescence quenching
Film sensor
Nitroaromatics
Aqueous phase

1. Introduction

The remarkable development of molecular and polymer electronics relies in a large extent upon the potential of organic material architectures to be tuned for improvement of color, band gap, morphology and other properties required for their optimal performance in specific applications such as chemical and biological sensing [1,2,3], emission [4,5] or storage of light [6]. Conjugated polymers are the paradigm of electronic organic materials and the subject of intense research endeavoring to tailor their luminescence and expand their fields of application [7]. In this context, an efficacious concept of macromolecular design aiming to customize the physical and electronic properties of conjugated polymers consists in the regular insertion in the polymer backbone of atomic or molecular motifs which tailor the π-conjugation length. Thus, a variety of regularly segmented conjugated polymers (SCPs) have been synthesized by linking aromatic segments of discrete size with spacers such as biphenylene [8], binaphthylene [9], paracyclophane [10], linear alkylene [11,12] and oxyethylene chains [13], oxygen atoms [14], silicon atoms [15,16] and sp^3-carbon atoms of the norbornylene [17], fluorenylidene [18] and isopropylidene groups [19-21] all of which break conjugation in a controlled manner.

In fact, the well-defined electro-optical properties of the aromatic segments are usually retained by the SCPs only in diluted solutions. In solid state, the aromatic units of SCPs often form inter-chain species that led to various morphological organizations at the molecular or nanoscopic level [12,13,22-24]. Thus, molecular anisometries, specific attractive forces and microsegregation often generates aggregates and excimers which have quite different electro-optical responses from those of the isolated unit in solution. The modification, and even degradation [23], of the photophysical properties of the chromophoric repeating units is an especially acute problem in SCPs with flexible spacers, whose conformational flexibility and amphilicity promote ordering of the anisometric rigid units [12,23]. But when the size of the spacer dwindles down to a single sp^3-carbon atom the gem-chromophores are forced into angular dispositions bringing forth twisted polymer microstructures which introduce a great deal of disorder into polymer morphologies. Therefore, in our studies we focused on the small isopropylidene spacer as the key element in designing regularly SCPs with amorphous morphologies which would ideally present optical properties insensible to the aggregation state. Thus, we were successful in obtaining polymeric amorphous assemblies of biphenylene [20], terphenylene [21], quaterphenylene [24] and diphenylfluorenylene [25] groups with good film-forming properties that are solution processable and each show similar optical responses either in solution or in solid state. Besides, despite the absence of side chains in the polymer architecture which is usually a condition to obtain soluble aromatic polymeric materials, we found that polymer solubilities are notably enhanced when the aromatic segments are tethered by the *meta* rather than *para* positions [25,26]; the same finding has been reported for quaterphenylenes linked with oligo(ethylene glycol) spacers [12]. Finally, the frustrated packing of semi-rigid segments causes void spaces that ease analyte exchange, thus making films of these nonaggregating amorphous luminescent materials good candidates for chemosensing by fluorescence quenching [1,3,25-28].

In this contribution, we describe the synthesis and report on the optical and chemosensing properties of two SCPs, **Pa** and **Pb**, in which the backbone consists of distyrylbenzene-based (DSB) moieties and isopropylene spacers (Scheme 1). The DSB family of chromophores displays excellent photophysical properties and has been the subject of intense research both as molecular materials [29-31] and as SCPs with flexible spacers [12,32-34]. However, the DSB groups tend to aggregate making their morphology at the molecular level highly dependent on subtle modifications of their structures. Thus, closely related members could arrange in different ground state aggregates, namely, J- and H-aggregates, the latter with π-stacking in either face-to-face and or in herringbone edge-to-face dispositions, all of them presenting their own optical signatures [29]; in addition, their excited states could form excited dimers. So, we decided to focus on the DSB chromophores partly because of its remarkable photophysical properties, and partly to test the effectiveness of the isopropylene spacer to yield polymeric amorphous assemblies of DSB chromophores, which could become a

good chemical sensing platform in the solid state. The related model compounds **Ma** and **Mb** were also synthetized (Scheme 1) and their optical and chemosensing properties were correlated with those of their parent polymers. The central benzene ring of the chosen DSB fluorophores for this study was either plain, **Ma** and **Pa**, or dimethoxy substituted, **Mb** and **Pb**, in order to find whether the increase in the electron-donor capacity of the electroactive aromatic segment was beneficial regarding their quenching performance with various hydrophilic and hydrophobic nitroaromatics. Because our main interest resides in environmental issues concerning detection of pollutants in soil and water bodies of city and industrial areas, the luminescence quenching response of thin films to NACs was evaluated mainly in aqueous solutions [35,36].

Scheme 1 (
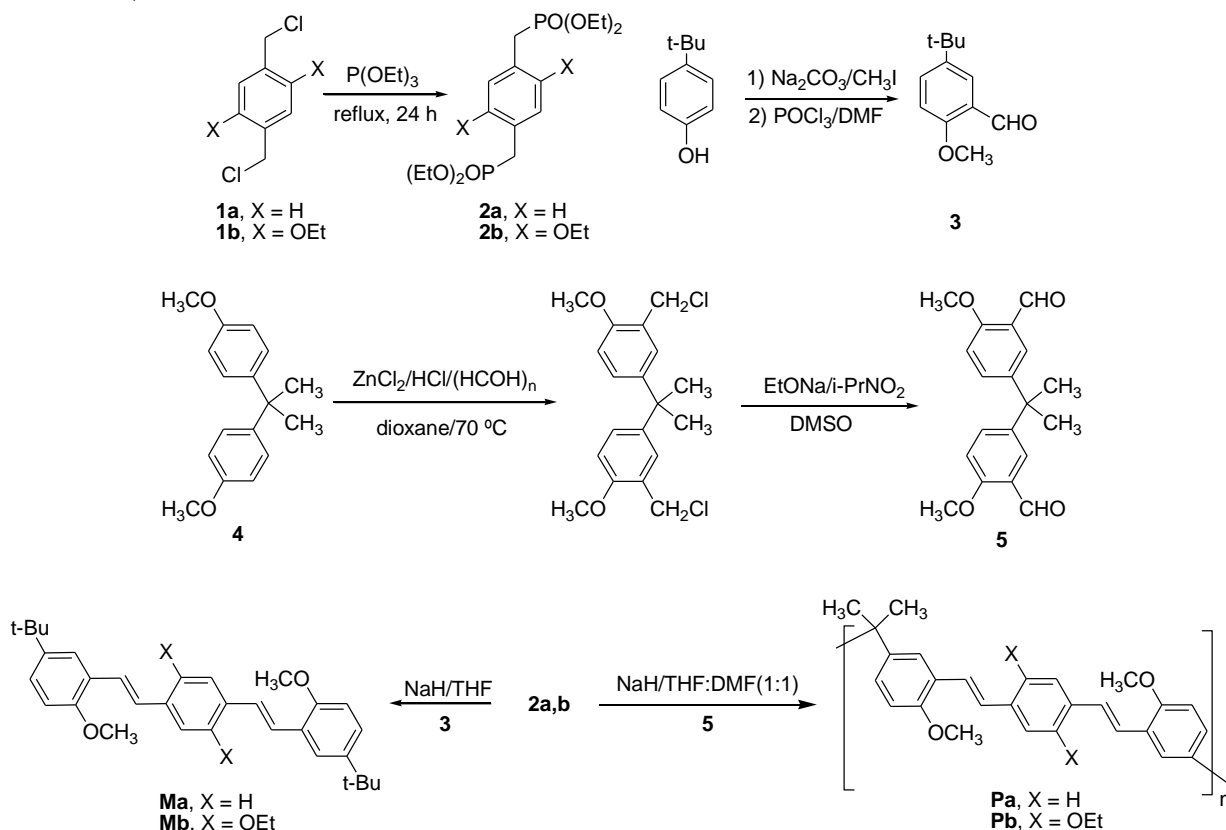
2. Experimental part

2.1 Materials

Reagents were purchased from Sigma and used without further purification unless otherwise specified. The solvents used for polymerization were purified by standard methods, thus THF was purified by distillation from Na/benzophenone while DMF was dried over molecular sieves and stored under Ar atmosphere. Chloroform used for spectroscopic measurements was of spectroscopic or equivalent grade.

2.2 Measurements and calculations

Melting points reported were not corrected. ^{1}H NMR (300 MHz) and ^{13}C NMR (75 MHz) spectra were recorded on a Bruker AVANCE III spectrometer at 25 °C. Chemical shifts are provided in ppm relative to TMS ($\delta = 0$ ppm) for ^{1}H and ^{13}C NMR. Elemental analyses (C, H) were performed in an EXETER CE-440 instrument at UMYMFOR (Argentina). FT-IR spectra were recorded on a FT-IR Nicolet spectrometer in KBr. Gel permeation chromatography analyses were carried out on THF solutions at room temperature using a Waters model 600 equipped with a Waters 2487 UV detector set at 254 nm. Calibration of the instrument was done using polystyrene standards. Thermal analysis was carried out on a TAQ20 instrument under nitrogen

flow. The scan rate was 5 °C/min. The thermal behavior was observed on an optical polarizing microscope (Leitz, Model Ortolux) equipped with a hot stage (Mettler).

UV/vis spectra were obtained from a UV-Visible GBC Cindra 20 spectrometer. The absorption measurements were done either on dilute samples (less than 0.01 g/ml) or on thin films cast on quartz plates, which were placed at a 30° angle with respect to the incident beam. Steady-state fluorescence studies were conducted using an SML AMINCO 4800 spectrofluorimeter at 25 °C. The emission measurements were carried out on dilute samples (less than 0.02 mg/ml) using a quartz cuvette with a path length of 1 cm and keeping the optical densities below 0.1 to minimize aggregation and reduce artifacts introduced by self-absorption in fluorescence. Thin film spectra were recorded by front-face (30°) detection. Film specimens were drop-cast from a $CHCl_3$ solution on quartz substrates and dried at room temperature. Fluorescence anisotropy was measured using a couple of film polarizers on the excitation and emission beams in the spectrofluorimeter operating in an L-format. The fluorescence anisotropy is calculated according to $‹r› = I_{vv} - GI_{vh}/(I_{vv} + G2I_{vh})$ where $I_{exc,em}$ is the intensity of the emission, v and h are the vertical or horizontal alignment of the excitation and emission polarizers, and $G = I_{hv}/I_{hh}$ is the instrumental correction factor which accounts for the difference in sensitivities for the detection and emission in the perpendicular and parallel polarized configurations.

2.3. Molecular Modeling

All calculations were performed with the ORCA program package (3.03 ed.) [37]. Pre- and post-processing operations were performed by using the graphical interface Gabedit 2.4.8 [38]. Structures were initially built graphically and optimized with the semi-empirical AM1 method. Molecular modeling of the model compounds and polymers was carried out using the HF-3c method [39]. This HF hybrid program use a small basis set MINIX, coupled with three empirical corrections, the atom-pairwise dispersion correction with the Becke-Johnson damping scheme (D3BJ) [40,41], the geometrical counterpoise correction gCP [42], and a short-ranged basis incompleteness correction, SRB. It was noted that the HF-3c yields rather flattened stilbene and DSB geometries quite similar to those obtained with DFT methods such as B3LYP/6-31G*. It was also found that for stilbene the B3LYP/def-SVP calculations coupled with the dispersion correction D3 and the basis set superposition error correction gCP gives a less planar conformation with dihedral angles of around 5-7° but still very far from the experimental value of 27°. Only a post-Harthree Fock method such as MP2 gives near experimental dihedral angles values. However, the computational cost of MP2 geometries is too high for our current purposes.

2.4 Fluorescence quenching studies

The films were cast onto carefully leveled quartz or glass substrates (2.4x0.8 cm) by spreading over the whole area 0.1 ml of a chloroform solution of the compound. The film was allowed to evaporate slowly in a nitrogen filled chamber and finally was kept under vacuum for 12 hours at room temperature. The thickness of cast films was measured in at least five different regions using a UV-visible interferometer (Model F20; Filmetrics, Inc.) operated in reflectance mode with a spot size of ~0.5 mm. Stock solutions (10^{-3} M) of each NAC were prepared by dissolving the adequate amount of the desired NAC in 3 mL of MeOH and by completing the volume up to 10 mL with water. Solid phase fluorescence quenching was investigated for the NACs at different concentrations on films whose thickness was *ca.* 200 nm for the polymers and *ca.* 50 nm for the model compounds. Quenching experiments were performed by inserting diagonally the films down to two-thirds of the height of the fluorescence cell. The 1 cm quartz cell was then filled with the solvent (2.4 mL) and spectra were acquired by front-face (30°) detection at room temperature after the addition of microliter aliquots of the quencher solution. Each fluorescence spectrum was recorded immediately after fluorescence intensity stabilization.

2.5 Synthesis

Bisphenol A (BPA) was recrystallised from ethanol prior to use. *Bis*(chloromethyl)benzene (**1a**) is commercially available. 1,4-*Bis*(chloromethyl)-2,5-diethoxybenzene (**1b**) was prepared from diethoxybenzene by chloromethylation according to the procedure of Wood and Gibson [43]. 2,2-bis(4-methoxyphenyl)propane (**4**) was prepared according to the literature [21].

The synthetic procedures are outlined in Scheme 1. The synthesis of the monomers started with the preparation of the bisphosphonates **2a** and **2b** which were obtained from the bischloromethylenes **1a** and **1b** using the Arbuzov reaction. Then, the monoaldehyde **3** was synthetized by formylation of the aromatic ring using the Vilsmeier-Haack reaction while the dialdehyde **5** was prepared in a sequence of two reactions from **4**. Thus, a mixture of **4**, formalin, $ZnCl_2$ and HCl afforded 2,2-bis(3-(chloromethyl)-4-methoxyphenyl)propane which after purification was treated with EtONa and nitro propane in DMSO to yield the dialdehyde **5**. Finally, the Wittig-Horner coupling of the bisphosphonates **2a** and **2b** with the dialdehyde **5** yielded the polymers **Pa** and **Pb**. Similar procedure, but using instead the monoaldehyde **4**, gave the model compounds **Ma** and **Mb**.

2.5.1 Synthesis of bisphosphonates **2a** y **2b**

Bisphosphonates were synthesized by a literature method [44] heating under reflux for 24 h a solution of the aromatic dichloride (24.0 mmol) in and triethylphosphite (50.4 mmol) under nitrogen atmosphere.

1,4-Bis(diethoxyphosphinylmethyl)benzene (**2a**) was recrystallized in cyclohexane to yield white plates. Yield: 73%; mp: 63-65 °C (lit. 75-76 °C) [45]. ^{1}H NMR (CDCl$_3$) δ: 7.25 (s, 4H), 4.00 (m, 8H), 3.12 (d, 4H, J_{H-P} = 20.4 Hz), 1.23 (t, 12H, J = 7.1 Hz). ^{13}C NMR (CDCl$_3$) δ: 130.3, 129.9, 62.1, 33.5 (J_{C-P} = 141.6 Hz), 16.3.

1,4-Bis(diethoxyphosphinylmethyl)-2,5-diethoxybenzene (**2b**) was recrystallized in cyclohexane to yield pale yellow needles. Yield: 65%; mp: 95-97 °C. ^{1}H NMR (CDCl$_3$) δ: 6.92 (d, 2H), 4.01 (m, 8H), 3.64 (c, 4H, J = 7.0 Hz), 3.25 (d, 4H, J_{H-P} = 20.2 Hz), 1.38 (t, 6H, J = 7.0 Hz), 1.24 (t, 12H, J = 7.1 Hz). ^{13}C NMR (CDCl$_3$) δ: 150.4, 119.7, 115.2, 64.6, 61.8, 26.4 (J_{C-P} = 140.3 Hz), 16.3, 14.9.

2.5.2 Synthesis of 2-methoxy-5-tert-butylbenzaldehyde (**3**)

DMF (33.2 g, 0.455 mol) was cooled at 0 °C and then POCl$_3$ (58.0 g, 0.378 mol) was added drop wise with agitation. The mixture was warmed at 35 °C and a solution of *tert*-butyl-4-methoxybenzene (3.0 g, 18.4 mmol) in 1,2-dichloroethane (30 mL) was added slowly. Afterwards, the mixture was stirred for 6 days at 35 °C. The reaction was quenched by addition of sodium acetate (50 mL) and water (100 mL) cooling at 0 °C, then extracted with CH$_2$Cl$_2$ (3x100 mL), dried with Na$_2$SO$_4$ and evaporated under reduced pressure. ^{1}H NMR (CDCl$_3$) δ: 10.5 (s, 1H), 7.85 (d, 1H, J_m =2.67 Hz), 7.58 (dd, 1H, J_m =2.67 Hz, J_o =8.77 Hz), 6.93 (d, 1H, J_o=8.77 Hz), 3.91 (s, 3H), 1.31 (s, 9H). ^{13}C NMR (CDCl$_3$) δ: 190.4, 160.3, 143.9, 133.4, 125.4, 124.7, 111.8, 56.1, 34.6, 31.8.

2.5.3 Synthesis of 2,2-bis(3-formyl-4-methoxyphenyl)propane (**5**)

First, to a solution of 2,2-*bis*(4-methoxyphenyl) propane (**4**) (9.56 g, 37.3 mmol) in dioxane (47 mL) was added powdered ZnCl$_2$ (5.0 g, 37.3 mmol). The stirred suspension was cooled to 5 °C and 35% HCl (5.03 g, 138 mmol) was added. The mixture was heated at 70 °C and 37% formalin (3.0 mL) was added. Additional 37% formalin was added (3 mL) when temperature reached 85 °C and then the mixture was then stirred for 8 h. After cooling at r.t., the organic layer was washed with NaHCO$_3$ (50 mL), water (3x50 mL), dried with Na$_2$SO$_4$ and the solvent was evaporated to yield 2,2-bis(3-(chloromethyl)-4-methoxyphenyl)propane as a white solid which was used as such in the next synthetic step. Yield: 13.5 g, 98 %. ^{1}H NMR (CDCl$_3$) δ: 7.21 (d, 1H ,J = 2.4 Hz), 7.12 (dd, 1H, J = 8.6, 2.4 Hz), 6.78 (d, 1H, J = 8.6 Hz), 4,61 (s, 2H), 3.85 (s, 3H), 1.64 (s, 3H). ^{13}C NMR (CDCl$_3$) δ: 155.3, 142.7, 128.8, 128.2, 125.0, 110.5, 66.9, 55.5, 41.8, 30.9.

To a stirred solution of Na (0.321 g, 13.6 mmol) in ethanol (19 mL) was added 2-nitropropane (1.92 g, 21.5 mmol) drop wise, then the emulsion was added to a solution of 2,2-bis(3-(chloromethyl)-4-methoxyphenyl)propane (2.00 g, 5.7 mmol) in DMSO (20 mL) under nitrogen atmosphere over a period of 10 min. The resulting mixture was stirred overnight and then quenched by addition of cold water (60 mL). The white solid was filtered off and dried in vacuo. Recrystallization from cyclohexane afforded **5**. Yield: 1.37 g, 77%; mp: 120-125 °C. ^{1}H NMR (CDCl$_3$) δ: 10.45 (s, 1H), 7.76 (d, 1H, J = 2.6 Hz,), 7.32 (dd, 1H, J = 8.8, 2.6 Hz,), 6.88 (d, 1H, J = 8.8 Hz,), 3.90 (s, 3H), 1.67 (s, 3H). ^{13}C NMR (CDCl$_3$) δ: 189.9, 160.2, 142.6, 134.8, 125.9, 124.2, 111.7, 55.7, 40.9, 30.6.

2.5.4 Synthesis of 1,4-bis(5-tert-butyl-2-methoxystyryl)benzene (**Ma**)

NaH 60% (0.125 g, 5.3 mmol) was washed 5 times with dry hexane under Argon atmosphere and suspended in dry DMF (2 mL). Then a solution of **1a** (0.295 g, 0.78 mmol) in dry DMF (2 mL) was added drop wise under Ar. The solution turned to greenish color. This mixture was stirred for 3 h and then a solution of **3** (0.30 g, 1.56 mmol) in dry DMF (3 mL) was added under Ar atmosphere. The solution was stirred at room temperature overnight, and quenched by the addition of water (3 mL) and HCl 5% (1.0 mL), extracted with CHCl$_3$ (3x10 mL), dried with Na$_2$SO$_4$ and evaporated *in vacuo*. The resulting solid was purified by column chromatography using CHCl$_3$ as eluent. Yield: 110 mg, 32%. ^{1}H NMR (CDCl$_3$) δ: 7.60 (d, 2H, J = 2.4 Hz), 7.52 (s, 4H), 7.48 (d, 2H, J = 16.5 Hz), 7.26 (dd, 2H, J = 8.5 Hz, J = 2.4 Hz), 7.12 (d, 2H, J = 16.5 Hz), 6.84 (d, 2H, J = 8.5 Hz), 3.88 (s, 6H), 1.35 (s, 18H). ^{13}C NMR (CDCl$_3$) δ: 155.0, 143.4, 137.2, 128.6, 126.8, 125.8, 125.5, 123.9, 123.6, 110.7, 55.7, 34.2, 31.6. FT-IR (KBr, cm^{-1}): 3050, 2963, 2853, 1251, 1980, 965, 807.

2.5.5 Synthesis of 1,4-bis(5-tert-butyl-2-methoxystyryl)-2,5-diethoxybenzene (**Mb**)

The procedure used for the model compound **Ma** (see above) was repeated for Mb with NaH (0.10 g, 2.48 mmol) in DMF (3 mL) and **1b** (0.269 g, 0.62 mmol) in DMF (3 mL). In this case the solution turned to reddish color. Then, **3** (0.25 g, 1.30 mmol) in DMF (3 mL) was added. Yield: 150 mg, 45%. mp: 145-146 °C. ^{1}H NMR (CDCl$_3$) δ: 7.55 (d, 2H, J = 2.3 Hz), 7.40 (s, 4H), 7.17 (dd, 2H, J = 8.6 Hz, J = 2.3 Hz), 7.09 (s, 2H), 6.76 (d, 2H, J = 8.6 Hz), 4.05 (c, 4H, J = 6.9 Hz), 3.79 (s, 6H), 1.40 (t, 6H,J = 6.6 Hz), 1.27 (s, 18H). ^{13}C NMR (CDCl$_3$) δ: 154.7, 151.0, 143.1, 127.5, 126.3, 125.1, 124.8, 123.7, 123.5, 111.3, 110.5, 65.3, 55.5, 34.0, 31.3, 14.9. FT-IR (KBr, cm^{-1}): 3060, 2962, 2866, 1248, 1053, 1032, 970, 810.

2.4.6 Synthesis of poly(2,2´´-dimethoxy-*p*-distyrylbenzene-5,5´´-ylene)propylene (**Pa**)

To a solution of **1a** (0.500 g, 1.32 mmol) in a 1:1 mixture of THF and DMF (6 mL) was added 60% sodium hydride oil dispersion (95 mg, 3.96 mmol) under nitrogen atmosphere. After cooling the mixture to 0 °C, a solution of **5** (0.413 g, 1.32 mmol) in 1:1 THF-DMF (6 mL) was added drop wise, then the reaction mixture was allowed to reach room temperature and stirred for 12 h at the same temperature. Afterward, a solution of the end-capping agent diethyl phenylphosphonate (15 mg, 0.066 mmol) in 1:1 THF-DMF (1.0 mL) was added and the mixture was stirred for additional 3 h. Benzaldehyde (14 mg, 0.132 mmol) in dry 1:1THF-DMF (1.0 mL) was then added, the mixture was stirred overnight. and then quenched with water (20 mL) and. After neutralization with HCl 35%, a yellow solid was obtained. The obtained polymer was purified by fractional precipitation from CHCl$_3$-methanol. Yield: 150 mg, 32%. ^{1}H NMR (CDCl$_3$) δ: 7.51 (d, 2H, J = 1.7 Hz), 7.48 (s, 2H), 7.44 (d, 2H, J = 16.5 Hz), 7.07 (dd, 2H J = 8.1 Hz, J = 1.7 Hz), 7.07 (d, 2H, J = 16.5 Hz), 6.79 (d, 2H; J = 8.5 Hz), 3.85 (s, 3H), 1.72 (s, 3H). ^{13}C NMR (CDCl$_3$, 5% DMF-d$_7$) δ: 154.9, 142.8, 137.1, 128.6, 127.2, 126.6, 125.5, 124.7, 123.6, 110.5, 53.3, 41.8, 31.0. FT-IR (KBr, cm^{-1}): 2990, 2950, 2830, 1255, 1120, 1036, 966, 806.

2.5.7 Synthesis of Poly(2,2´´-dimethoxy-2´,2´-diethoxy-*p*-distyrylbenzene-5,5´´-ylene)propylene (**Pb**).

The procedure used for polymer **Pa** (see above) was repeated for **Pb**. **1b** (0.500 g, 0.92 mmol) in dry THF-DMF 1:1 (7 mL), sodium hydride (0.066 g, 2.76 mmol), **5** (0.287 g, 0.92 mmol) in 6 mL THF-DMF (1:1).

Diethyl phenylphosphonate (0.010 mg, 0.046 mmol) in dry THF-DMF 1:1 (1.0 mL), benzaldehyde (0.010 g, 0.092 mmol) in dry THF-DMF 1:1 (1.0 mL). Yield: 184 mg, 43%. ^{1}H NMR (CDCl$_3$) δ: 7.54 (d, 2H, J = 1.3 Hz), 7.12 (s, 2H), 7.42 (s, 4H), 7.07 (dd, 2H J = 8.7 Hz, J = 1.3 Hz), 6.79 (d, 2H, J = 8.7 Hz), 4.07 (c, 4H, J = 6.8 Hz), 3.85 (s, 3H), 1.72 (s, 3H), 1.42 (t, 6H, J = 6.8 Hz). ^{13}C NMR (CDCl$_3$, 5% DMF-d$_7$) δ: 154.9, 151.0, 142.9, 127.4, 126.9, 126.1, 124.9, 123.9, 123.8, 111.2, 110.4, 65.3, 55.4, 41.8, 30.9, 14.9.FT-IR (KBr, cm^{-1}): 3050, 2961, 2831, 1246, 1186, 1028, 973, 819.

3. Results and discussion

3.1 Synthesis

The synthetic routes used to obtain model compounds **M** and polymers **P** are shown in Scheme 1. First, the bisphosphonates **2a,b** were prepared in almost quantitative yields from the corresponding bischloromethylene compounds **1a,b**. Then, the synthesis of the monoaldehyde **3** was attempted using standard Vilsmeier-Haack reaction conditions with 2 equivalents of POCl$_3$ in DMF, but to obtain only traces of **3**. However, the use of a large excess of the reagent (1:20) and very long reaction times afforded **3** in 67% yield after chromatographic purification. Finally, the model compounds **Ma** and **Mb** were synthesized by Wittig-Horner coupling between **3** and bisphosphonates **2a** and **2b**. A trans configuration was assigned to these model compounds by ^{1}H NMR and FTIR. Thus, **Ma** presents coupling constants of vinylic protons (J_{trans}) of *ca.* 16 Hz. In addition, both **Ma** and **Mb** show intense bands in the 960 cm^{-1} region which corresponds to the out-of-plane deformation band in trans carbon-carbon double bonds. Due to the poor performance of the Vilsmeier route in the direct diformylation of **4**, the key dialdehyde monomer **5** for copolymerization with the bisphosphonates was instead obtained by chloromethylation followed by oxidation with an overall yield of 75%.
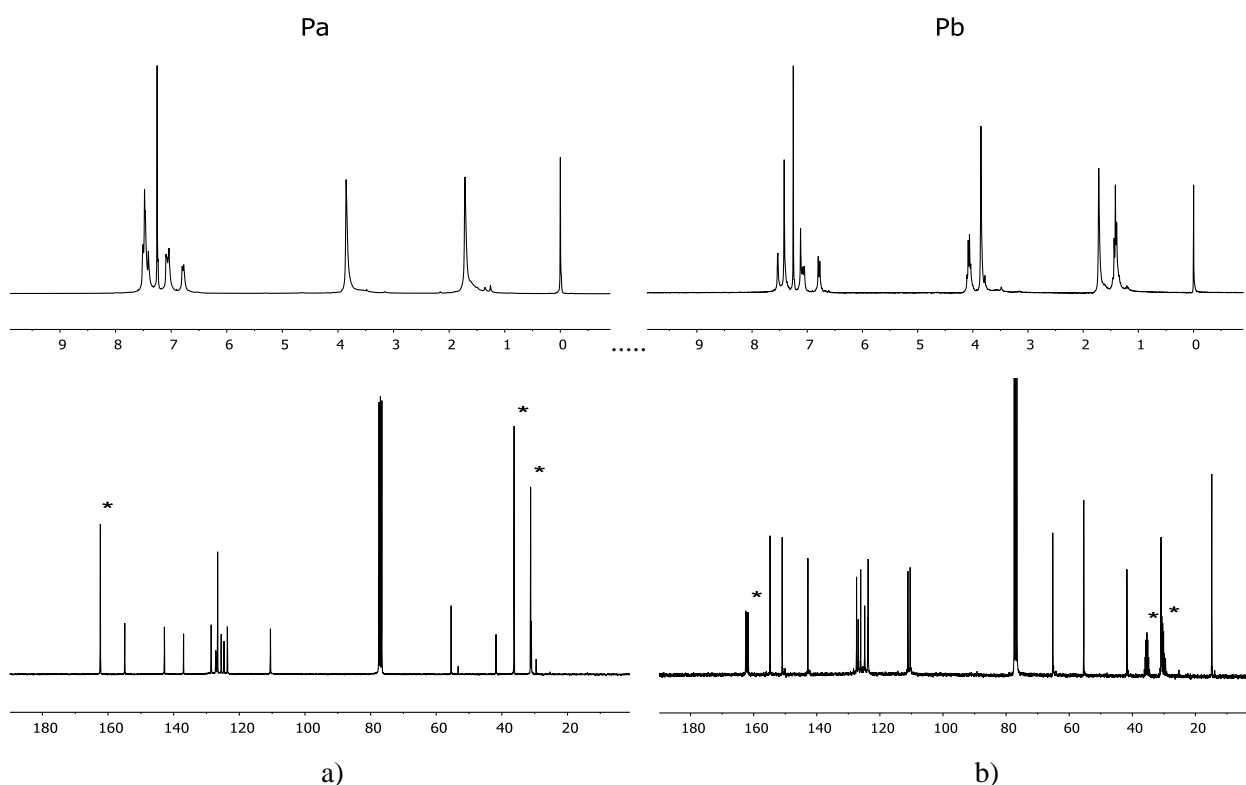

Figure 1. a) [1]H(CDCl$_3$) and ^{13}C NMR(CDCl$_3$ with 5% DMF) spectra of polymer **Pa** . b) [1]H(CDCl$_3$) and ^{13}C NMR(CDCl$_3$ with 5% DMF-d$_7$) spectra of polymer **Pb**. * [13]C signal from either DMF or DMF-d$_7$.

The new segmented conjugated polymers **Pa** and **Pb** with *meta*-linked bis(styrylarylene) units were synthesized using the Wittig-Horner reaction with yields of 30-60% after repeated reprecipitations. We

observed that the polymers precipitated in the reaction media when THF was used as solvent. In contrast, polymers obtained in THF:DMF (1:1) reaction mixtures remained soluble throughout the entire reaction without precipitation or gel formation and consistently gave higher degrees of polymerization (DP_n). Polymerizations were terminated by addition of diethyl benzylphosphonate and benzaldehyde as end-capping agents and the as-made polymers were purified by fractional reprecipitation from CHCl$_3$-methanol. **Pa** and **Pb** were soluble in a variety of organic solvents like CHCl$_3$, CH$_2$Cl$_2$, DMF, toluene or THF despite the absence in their backbone of solubilizing long chains. Gel permeation chromatography (GPC) indicated that relatively medium to high number average molecular weights were achieved (**Pa**, M_n = 30.0 kDa, M_n/M_w = 2.1, DP_n = 78; **Mb**, M_n = 11.4 kDa, M_n/M_w = 2.1, DP_n = 23). The ^{1}H and ^{13}C NMR spectra indicated that both polymers **P** have high structural homogeneity with an all-trans stereochemistry (Fig. 1). Polymers **Pa** and **Pb** showed coupling constants of *ca.* 16 Hz and an intense IR band at $\approx$ 960 cm^{-1}, that is, similar to those observed for their corresponding model compounds

3.2. Morphology. Thermal and optical studies.

The new distyrylbenzene model compounds are highly soluble light yellow powders. The DSC trace on Fig. 2 of **Ma** showed a crystallization exotherm at 42 °C, a weak glass transition at 66 °C followed by a broad melting that occurs in the 140-180 °C range, that is, approximately 100 °C lower than that of its unsubstituted parent 1,4-bis[(E)-2-phenylvinyl]benzene (264-266 °C) [46]. **Ma** shows strong supercooling of about 130 °C before the broad transition around 46 °C sets in. The model compound with ethoxy substituents, **Mb**, presents a supercooling of 90 °C and a more defined crystallization exotherm than that of **Ma** (Table 1). Hence, **Mb** is less prone to form disordered assemblies than **Ma**. Thus, the overall thermal behavior of model compounds can be traced to the presence of bulky t-butyl groups which are known to hinder crystallization in bis(styryl)arylenes [29]. Although bulk samples of **Ma** and **Mb** do not give kinetically stable amorphous phases, transparent homogeneous thin films, with thickness ranging from 20 to 200 nm, casted from chloroform solutions were suitable for optical measurements.
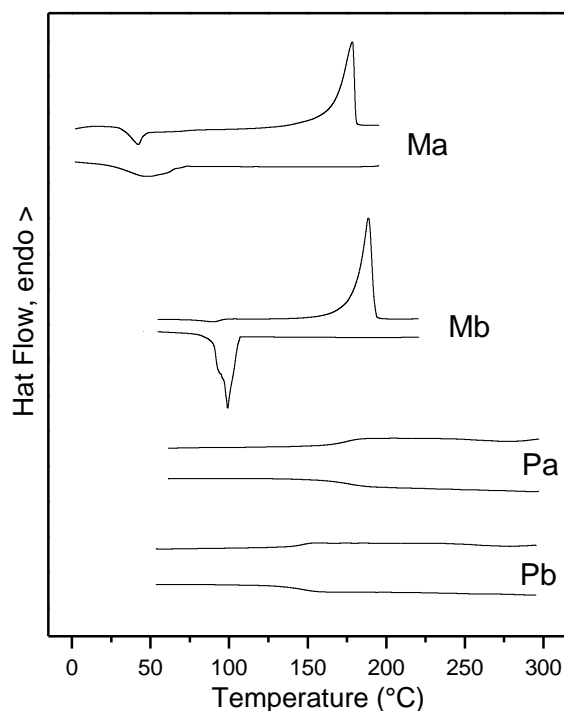

Figure 2. DSC traces of model compound **Ma** and **Mb** and polymers **Pa** and **Pb**.

Furthermore, thicker films remained transparent with no birefringence detected by POM observations even after several weeks. According to evidence from DSC and POM experiments polymers **Pa** and **Pb** are

amorphous; their DSC traces registered at a temperature range between 50 and 300 °C showed only distinct glass transitions and no melting transitions were found upon heating beyond the glass transition temperature (Table 1 and Fig. 2). Moreover, birefringent textures were not observed either for **Pa** or **Pb** during POM experiments carried out in the same temperature range. Both polymers easily gave smooth thin films casted on quartz plates. These findings are consistent with our current thinking that the forced angular disposition of the gem-chromophores linked by a single sp3-carbon atom brings about highly distorted main chains that hamper ordering processes [21]. The twisted nature of **Pa** is highlighted by the HF-3c molecular model of the tetramer shown in Fig. 3a.

The macroscopic information from DSC and POM analysis was coupled with the results acquired using spectroscopic methods which can provide information about local ordering of the chromophores. The optical absorption is a highly localized process which samples the entire diversity of absorbing species within the film, and as such it indicates disorder much more than emission will. On the contrary, excitations usually move across the chromophoric assembly by resonance energy transfer processes to finally emit from sites for which the energy of the excited state is smallest; therefore emission usually occurs from a single species. This delocalization is also relevant for our sensing studies because exciton migration boost its interaction with quenchers thus improving detection sensitivity. Therefore, bearing in mind both film characterization and sensing applications, energy migration in the thin films was evaluated by fluorescence depolarization measurements which yielded low residual values of the steady-state anisotropy in the range of <r> ~ 0.05 - 0.09 (Table 1), thus indicating good exciton mobility in model compounds **M** as well as in polymers **P**.

a)

b)   c)
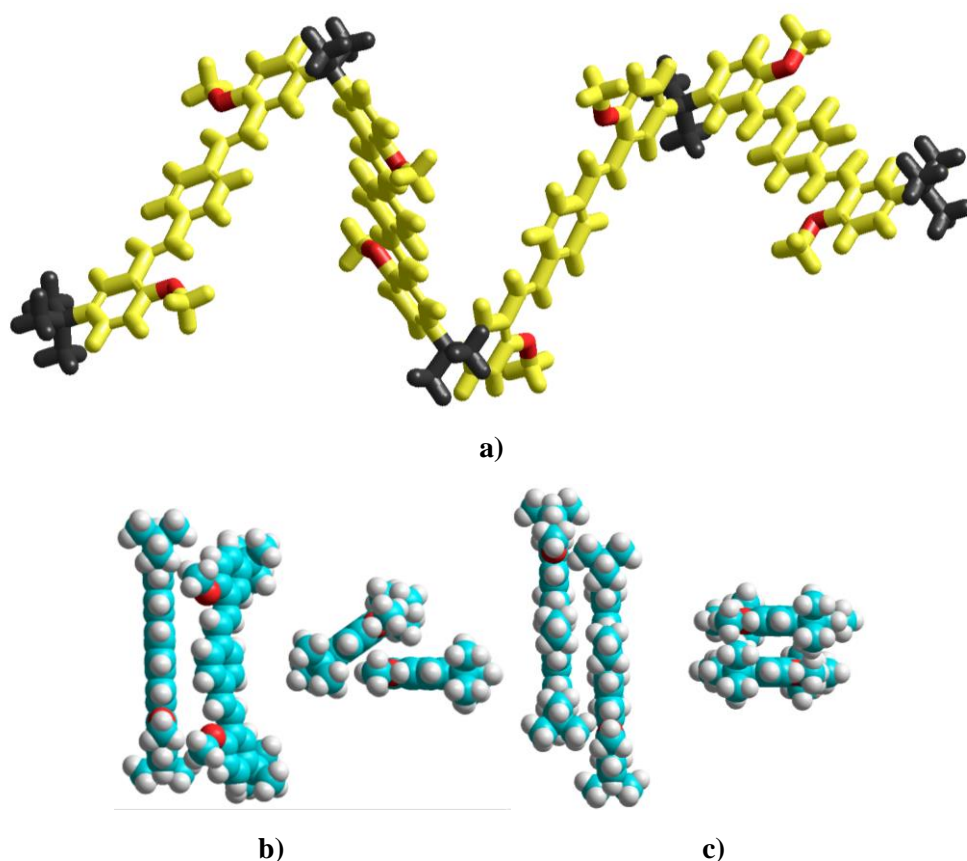
Figure 3. a) HF-3c relaxed geometry of a tetramer of **Pa**, the isopropylidene linking group and the two end-capping t-butyl groups are shown in black. b) A representation of a herringbone H-arrangement of **Ma** is shown in a side view (left) and a front view (right). b) A representation of a J-arrangement of **Mb** is shown in a side view (left) and front view (right).

Table 1. Thermal and photophysical properties of model compound **Ma,b** and polymers **Pa,b**.

	DSC[a]		Abs.			Fluo.			
	Tg	Tm, Tc	media[b]	λ_{max}[c] A_2, A_1	f_{whm}[d]	λ_{max}[e] E_1, E_2	fwhm[f]	SS[g]	‹r›[h]
Ma	66	178, 46(broad)	CHCl$_3$	310, **369**	4810	416, **439**	3120	3060	-
			film	313, **383**, 414	8540	437, **462**, 492	2650	1270	0.064
Pa	175	-	CHCl$_3$	312, **364**	7580	422, **444**, 468	3200	3780	-
			film	317, **378**	7550	427, **452**	4410	2930	0.069
Mb	-	189, 99(broad)	CHCl$_3$	319, **391**	4470	**453**, 481	2500	3500	-
			film	368, **422**, 468	10930	513	2650	1870	0.055
Pb	155	-	CHCl$_3$	318, **394**	4860	**458**, 483, 526	2430	3550	-
			film	328, **400**	6630	524	2780	5920	0.087

[a] Determined by DSC at scan rates of 5 ºC/min, in ºC. Tg = Glass transition temperature and Tm = melting temperature from second heating cycle, Tc = crystallization temperature from first cooling cycle.
[b] Measured from dilute CHCl$_3$ solutions and pristine thin films.
[c] Absorption maxima measured in dilute CHCl$_3$ solutions and on films, bold data indicate the major peaks.
[d] Full width at half-maximum of the absorption bands (in cm^{-1}).
[e] Emission maxima measured in dilute CHCl$_3$ solutions and on films. Bold data indicate the major peaks.
[f] Full width at half-maximum of the fluorescence bands (in cm^{-1}).
[g] Stokes shifts in dilute CHCl$_3$ solutions and on films ($\lambda_{E1} - \lambda_{A1}$ in cm^{-1}).
[h] Average anisotropy measured in thin films in an emission range of 60 nm around the $\lambda_{max,em}$.

Optical studies in distyrylbenzenes have been most useful in characterizing their polymorphism in solid state [29]. In particular, comparison of the solution and solid state optical data often provide insight into the multiple environments that could be present in the solid state. Shown in Fig. 4 are the normalized UV-vis and fluorescence spectra of **Ma**, **Mb**, **Pa** and **Pb** in solutions and thin films. The absorption and emission data is listed in Table 1. Fig. 4a compares the absorption and emission spectra of the model compound **Ma** and polymer **Pa** in dilute chloroform solution. Same data is presented for **Mb** and **Pb** in Fig. 4b. The maxima, vibronic structure with a prominent A_1 absorption transition peak and two distinct emission bands, E_1 and E_2, full width at half-maximum (FWHM) of the absorption and fluorescence bands and stokes shifts of **Ma** and **Pa** on one side and **Mb** and **Pb** on the other are quite similar in solution (see also Table 1), thereby arguing for the effective electronic isolation of gem-chromophores by isopropyl groups in the polymer main chain [21,25].
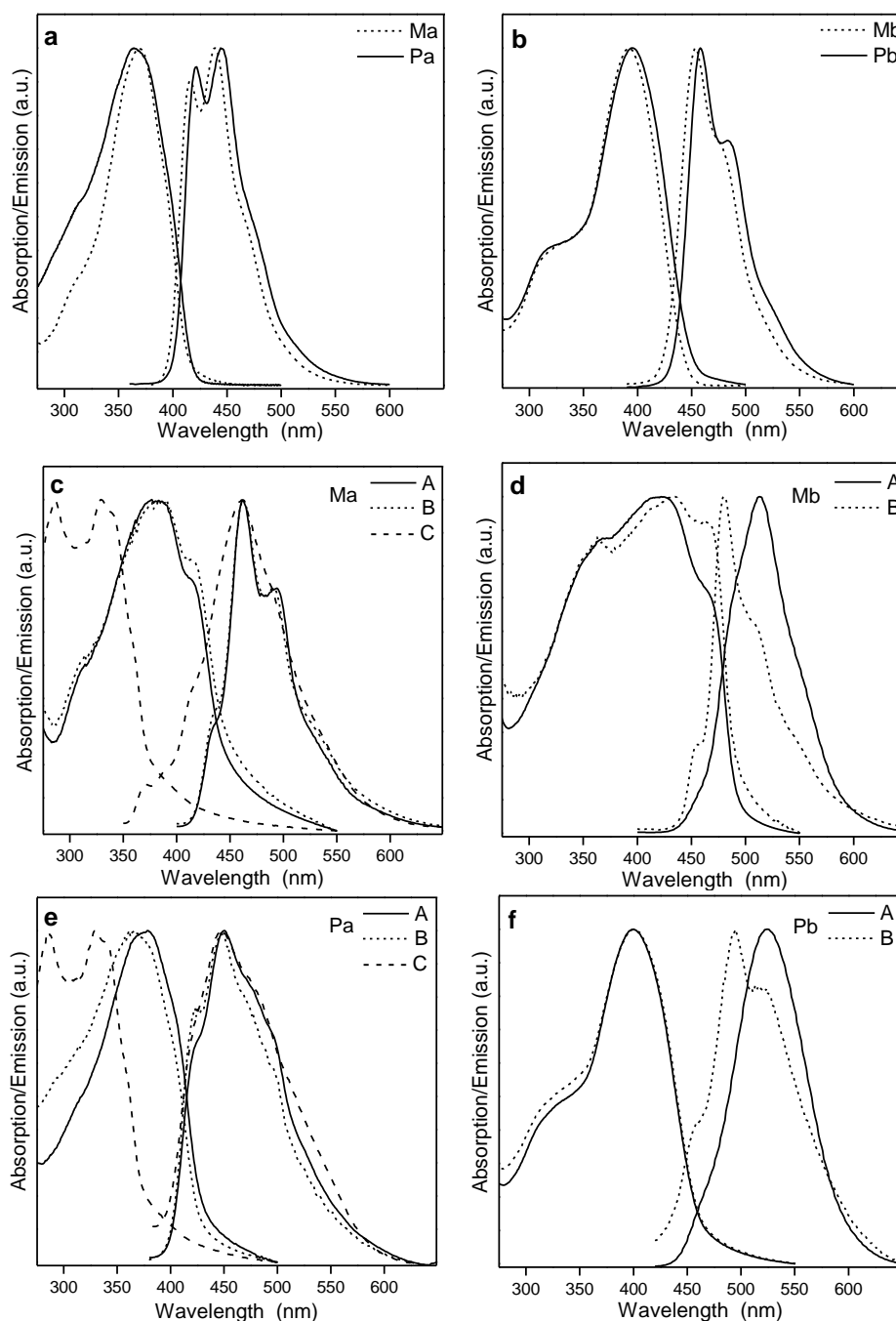
Figure 4. a) Absorption (left) and emission (right) spectra. CHCl$_3$ solutions of a) **Ma** and **Pa** and b) **Mb** and **Pb**. Pristine (A), annealed (B) and aged (C) thin films of b) **Ma**, d) **Mb**, e) **Pa** and f) **Pb**.

Spectra in the solid state were recorded periodically from the pristine films, then after mild annealing at 50 °C for 3 h under vacuum, and finally after annealing for 2 h under nitrogen at 100 °C in the case of the model compounds and at 180 °C for the polymers. Spectra were also recorded from the as-made films after an extended storage period of 10 months at room temperature in the dark. In another experiment, the pristine films were immersed in water while the spectra of the hydrated films were measured for up to 24 hours. Fig. 4c and 4e illustrate the optical spectra of **Ma** and **Pa** from pristine films (A) and after mild annealing at 50 °C (B). No significant spectral variations were observed between spectra recorded from films annealed initially at 50 °C and then at higher temperatures. The absorption and fluorescent spectra of as-made films of **Ma** and **Pa** show no distinctive differences against those in solution, in fact, they are only slightly red-shifted. These bathochromic shifts appear to be due mainly to the moderate isotropic polarizability of a disordered assembly

11

of chromophores similar to those observed in other amorphous tert-butyl substituted DSBs [29,47]. The spectral similarities indicate first the absence of strong interactions between neighboring chromophores in the solid state and second that similar disordered assemblies are bring about either by the bulky tert-butyl groups present in **Ma** or the twisted main chain of **Pa**. Other common features shared by **Ma** and **Pa** films are that annealing as well as water solvation caused only slight spectral variations. Although hydration smoothed the vibronic pattern of emission the λ_{max} change very little, in fact, λ_{max}(solution) = 439 nm ≈ λ_{max}(pristine) = 462 nm ≈ λ_{max}(hydrated) = 439 nm for **Ma** and λ_{max}(solution) = 444 nm ≈ λ_{max}(pristine) = 449 nm ≈ λ_{max}(hydrated) = 451 nm for **Pa**. However, a blue-shift of the absorption and a broadening in the emission were observed in the aged films after a ten month storage period (see trace C in Fig. 4c and 4e) which indicate that modifications in molecular segmental arrangements sluggishly occurred at room temperature leading to better ordered domains within the overall amorphous films. It is worth mentioning that, in DSB-type compounds, distinct blue-shifts of the main absorption band and moderate red-shifts in the emission band in going from solution to condensed phase are optical signatures of H-type aggregation with edge-to-face arrangement of parallel adjacent molecules [47]. This herringbone organization prevents the strong intermolecular vibronic coupling between chromophores that in π-stacked H-aggregates leads to large red-shifted excimer-like emission spectra and to very low luminescence intensities. The spatial arrangements of two HF-3c geometries of **Ma** depicted in Fig. 3b shows that the herringbone alignment could be accomplished for at least some of the rotamers of DSB chromophores with two t-butyl groups in meta positions forming weak H-aggregates, while it has been observed that this organization is very difficult to achieve when there are four t-butyl groups [29,48].

The EtO substitution in the central aromatic ring produces in solution a modest ~ 30 nm red shift in both absorption and emission spectra of **Mb** and **Pb** against those of **Ma** and **Pa**. However, this substitution brings more pronounced modifications of the optical behavior in solid state. Thus, the absorption spectrum of a pristine film of **Mb** is red-shifted against that in solution and shows an increase in the A_1/A_2 ratio while the emission spectrum presents an almost unstructured band with a λ_{max} shifted about 80 nm from the value observed in solution and a decrease in the E_1/E_2 ratio (Table 1, Fig. 4d). Such variations in the A_1/A_2 and the E_1/E_2 ratios are usually attributed to an increase in molecular order [49]. The large broadening of the absorption band points to the formation of aggregates in the pristine films while the unstructured and moderately red shifted emission band suggest that emission comes mainly from weak H-aggregates similar to those observed in **Ma**. The shape of the emission band of **Mb** is highly dependent on the casting conditions, type of substrate and temperature. Moreover, it is noticeable in Fig. 4d the small Stoke´s shift due to the increased A_1/A_2 ratio and red-shift of the absorption and the blue-shifted emission observed after annealing, which produced a vibronically structured emission with λ_{max} at 481 nm and shoulders at 454 and 509 nm. Therefore, after mild annealing the films modified their spectral features which then resemble more closely the ones observed in alkoxy co-substituted DSBs for aggregates organized in a J-type disposition which consists in the slip-stacked parallel alignment of neighboring chromophores [29,48]. Such spatial organization is illustrated in Fig. 3c for a chromophore J-aggregate formed from two HF-3c geometries of **Mb**. Indeed, the same blue shift of the emission band can also be induced by immersing the pristine film in water. Although the diffusion of water molecules into a film usually increases molecular reorientations as well as the polarity of the excited state environment, more probably this blue shift is originated from a morphological modification that change the population ratio of the emitters from H- to J-aggregates due to increased rotational and conformational mobility since the same optical shift was brought about by the thermal treatment. On the other hand, and in contrast with **Ma**, the long term storage do not seems to increase local order already present in **Mb** films, as the absorption and emission spectra registered after 10 months are similar to those obtained from pristine films (not shown). On the contrary, absorption spectra of pristine films of the amorphous polymer **Pb** (Fig. 4f) closely follow the ones recorded in dilute solution but they are markedly different from those of **Mb** recorded in solid state. Interestingly, no changes in the polymer

absorption are produced by thermal treatments or hydration. However, the unstructured red-shifted emission band of **Pb** is similar to that observed in **Mb**. So, although the absorption features suggest that the local order in **Pb** is much reduced in comparison with **Mb**, the nature of the low energy emission species in both compounds seems to be quite similar. Likewise, the thermal treatment of **Mb** and **Pb** films yield in both cases a new blue-shifted structured emission band at *ca.* 480 nm with the coincident disappearance of the original band (see Fig. 4d and 4f). But, though the same blue-shift occurred on hydration in **Mb** films, the hydrated films of **Pb** retained the ~ 530 nm original emission band. In summary, thin films of **Ma** and **Pa** showed closely related spectral features. But the EtO-substitution enhances the interchromophoric electronic interactions in **Mb** that can only be overcome in **Pb** by the contorted polymeric main chain. In addition, the EtO-substitution generates blue-shifted emitting species whose fate depends on the structural capacity of the material to retain the original arrangements in the pristine film. The tendency of DSB moieties to form aggregates in the model compound and the fluctuating appearance of the emission band on the casting conditions is greatly diminished by this polymeric architecture. The isotropic disposition of chromophores in polymer films is stabilized to such an extent that thermal annealing has no effect in increasing the overall order. Indeed, solutions and pristine, annealed or hydrated thin films of **Pa** showed similar absorption and emission spectra. The same behavior is seen for solutions and pristine or hydrated films of **Pb**.

3.3. Fluorescence quenching studies with NACs in hydroxylic media

Next, the sensing properties of these DSB-materials were evaluated since the morphological and optical properties indicate that they could present good performances as fluorescent sensing platforms.The steady-state quenching experiments were performed in the solid state on highly fluorescent thin films immersed in a hydroxylic solvent. This sensing configuration involves interchange between the film and its bathing of mobile species (solvent and analytes) and their subsequent interactions of electronic nature with excitons and of cohesive character with the organic environment in the film interior. The films were casted onto dodecyltrichlorosilane, DTS, coated glass substrates. We have found previously that the insertion of a monolayer of nonpolar aliphatic chains between the organic sensing layer and the glass substrate, which largely reduce the solvent affinity for the surface, improve adhesion and the physico-mechanical stability of the organic film [28]. Moreover, the presence of the nonpolar layer was decisive in producing transparent films of **Mb** and, to a lesser degree, of **Ma** which in general showed lesser tendency to form opaque films. Fluorescence control experiments on films of the model compounds indicated that there was no leakage from the film towards water media after 24 hours. However, increasing levels of fluorescence were observed in the solvating media when the films were immersed in H_2O/MeOH (1:1) or pure MeOH. No leakage was detected for the polymer films in H_2O, H_2O/MeOH (1:1) mixture or plain MeOH. Pristine films were immersed in the hydroxylic solvent and allowed to solvate prior to record their steady-state fluorescence response to increments in the concentration of various hydrophilic (i.e.: 4-nitrophenol, NP; 2,4-dinitrophenol, DNP; 2,4,6-trinitrophenol, TNP) and hydrophobic (i.e.: 4-nitrotoluene, NT, 2,4-dinitrotoluene, DNT; 2,4,6-trinitrotoluene, TNT) nitroaromatics.

Fluorescence quenching was fast, complete and reversible showing that analytes diffuse easily into the DSB-based films. The reversibility of the sensing response was studied by quenching-recovery experiments. Thus, a solvated film of **Pa** was first exposed to a large concentration of the quencher for about one minute which was then removed with care and the film washed twice with water. This procedure was repeated several times. The fluorescence responses in the presence and absence of the quencher plotted in Fig. 5a show that the quenching of the fluorescence was a reversible process. Thus, even after six cycles the film showed near complete quenching and fluorescence recovery. Same experiment was repeated for **Pb** though in this case fluorescence was measured twice, first after one and then after five minutes (Fig. 5b). No further decrease in the fluorescence was observed at the longer time thus corroborating that quenching was quick.
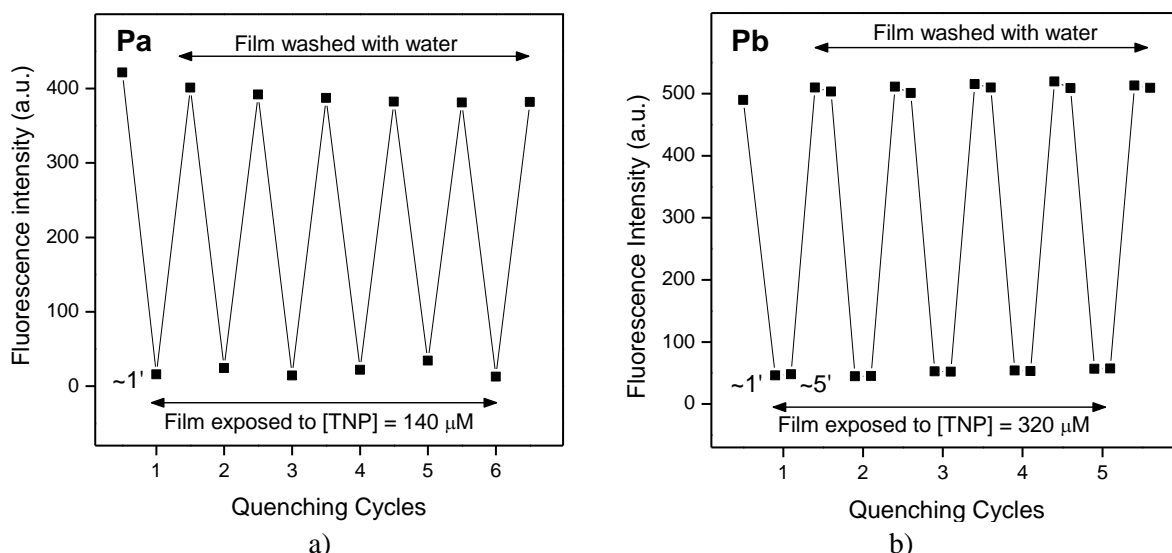
Figure 5. a) Six continuous cycles of quenching-recovery test of a film of **Pa**. The quenching was measured after exposing the film to [TNF] = 1.4 10^{-4} M for ~ 1 min ($\lambda_{ex}/\lambda_{em}$ = 379/451 nm). b) Five continuous cycles of quenching-recovery test of a film of **Pb**. The quenching was measured after exposing the film to [TNF] = 3.2 10^{-4} M for ~ 1 min and ~ 5 min ($\lambda_{ex}/\lambda_{em}$ = 430/532 nm).

Fig. 6 displays the quenching of the emission spectrum of thin films of **Pa** and **Pb** in water upon addition of microliter aliquots of NACs. The plots of the Stern-Volmer (S-V) equation, (I_o/I) -1 = K_{SV} [Q], for fluorescence quenching are shown in Fig. 5a (inset) and Fig. 5b (inset). The S-V constant (K_{SV}) and the values of half of the maximum quench, $Q_{50\%}$, that is, the quencher concentration needed to reach (I_o/I) - 1 = 1 of polymer and model compounds are shown in Table 2.
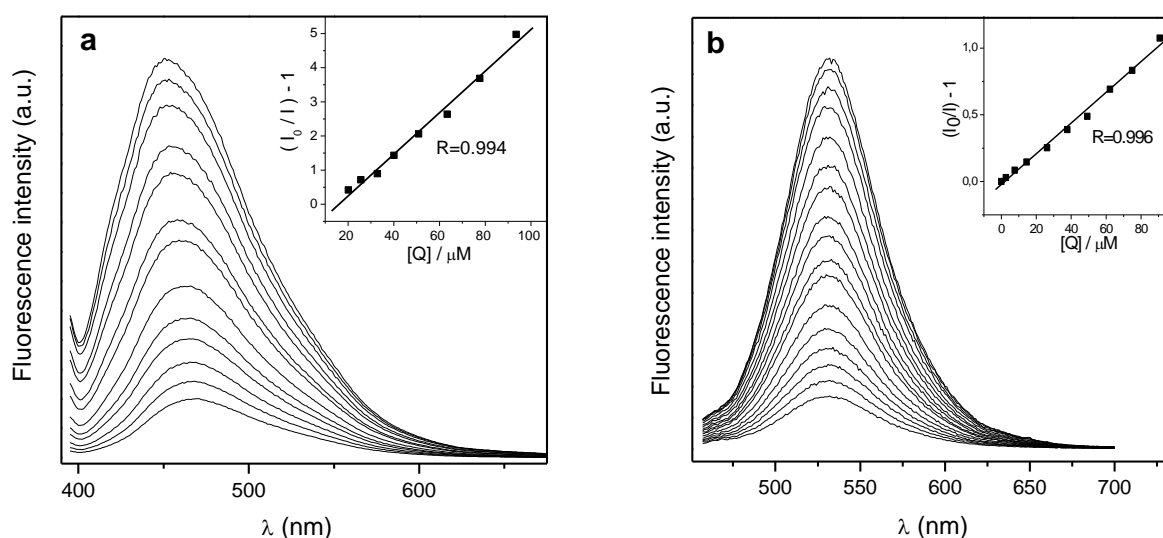

Figure 6. a) Fluorescence spectra change (λ_{ex} = 379 nm, λ_{em} = 451 nm) of a **Pa** film as a function of added TNP in water; [TNP] = 3.7 10^{-6} – 1.1 10^{-4} M (top to bottom). b) Fluorescence spectra change (λ_{ex} = 430 nm, λ_{em} = 532 nm) of a **Pb** film as a function of added TNP in water; [TNP] = 2.5 10^{-6} – 2.6 10^{-4} M (top to bottom). The Stern-Volmer plots for the linear region are shown in the insets.

Linear S-V relationships (R^2 > 0.99) were observed model compound and **Pa** for most the NACs tested even though only in the range ~20-30 to ~65-70% of fluorescence quenching. **Pb** showed linear relationships in narrower ranges with less satisfactory correlation coefficients ($R^2 \geq 0.98$). A non-linear S-V relationship with upward curvature usually occurred at the higher end of quencher concentrations for the polymers (Fig. 6a) while the model compounds showed a more linear behavior. The non-linear response observed as the

analyte concentration increases is most probably because of increasingly efficient quenching of migrants excitons [2,28]

Table 2. Data analysis of Stern-Volmer plots and quenching efficiencies

Quencher (Q)	Solvent	K_{SV}, M^{-1}	$Q_{50\%}$,[a) μM	K_{SV}, M^{-1}	$Q_{50\%}$,[a) μM
		Ma		**Mb**	
TNP	H_2O	97900	9.9	80200	20
TNT	H_2O	17400	60	18100	63
		Pa		**Pb**	
NP	H_2O	5920	170	-	-
DNP	H_2O	41900	47	-	-
TNP	H_2O	60900	34	12500	90
TNP	MeOH	23200	37	11100	110
NT	H_2O	8500	120	-	-
DNT	H_2O	3040	200	-	-
TNT	H_2O	[b)	570	[b)	1100
TNT	MeOH	940	970	3540	640

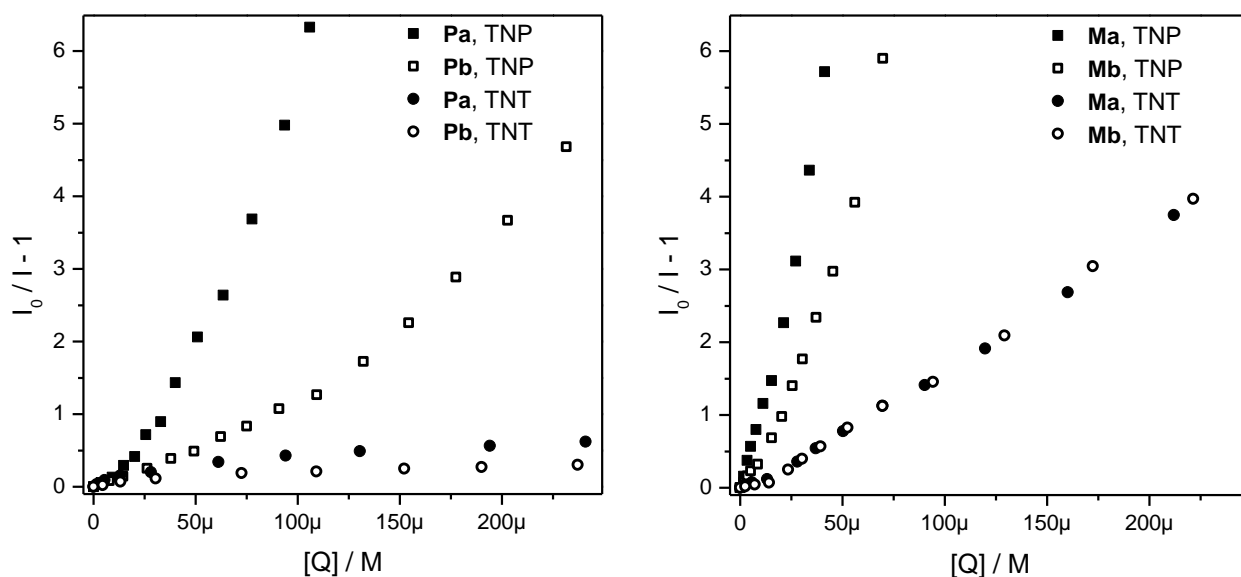[a] [Q] for $(I_o/I) - 1 = 1$. [b) Non-linear S-V relationships.

Figure 7. Stern-Volmer plots of polymers and model compounds in response to TNP and TNT.

Since the development of small molecule fluorescent sensors is an intense field of research [50], we also tested the model compounds in the quenching studies and their quenching efficiencies were correlated with those of their parent polymers. All compounds tested in this study are much more sensitive to TNP than to TNT in aqueous media (see Fig. 7). It also was found that **Pa** and **Ma** showed higher overall quenching efficiencies than **Pb** and **Mb** despite the fact that **Pb** and **Mb** have better electron-donating capabilities because of the diethoxy substitution. In fact, the efficiency ratio for TNP is $Q_{50\%,\text{Pa}}/Q_{50\%,\text{Pb}} \approx 3$ while for TNT is $Q_{50\%,\text{Pa}}/Q_{50\%,\text{Pb}} \approx 2$. This outcome cannot be rationalized in terms of electronic considerations based on the accepted mechanism of fluorescence sensing of NACs that consists of the photo-induced electron transfer from an electron-rich chromophore to an electron-deficient NAC. Moreover, the results with a series of

quenchers with increased electron-deficiency are contradictory, while quenching efficiencies for **Pa** increase with the number of nitro group for the hydrophilic nitrophenols (TNP > DNP > NP), the opposite was observed with the hydrophobic nitrotoluenes (NT > DNT > TNT). However, the presence of as least one strongly electron accepting nitro group in the aromatic ring of the analyte was required to achieve acceptable quenching efficiencies of the emission of the electron-rich polymer **Pa**. Thus, either the parent compounds lacking nitro groups, i.e.: phenol and toluene, or the diphenolic compounds such as hydroquinone, HQ, or 1,5-dihydroxynaphtalene, DHN, which have two electron donating groups produced only very slight negative (toluene,phenol and HQ) or positive (DHN) responses which were from two to three orders of magnitude smaller than the one observed for TNP (see Fig. 8). Additionally, we tested the response of **Pa** films in aqueous media against other chemicals which are normally found in industrial wastewaters [51,52]. These chemicals could act as interferents and alter the detection of NACs. It is therefore important to assess the selectivity of these polymers toward NACs. No significant change in **Pa** fluorescence was detected by exposition to micromolar quantities of several possible interferents (Fig. 8). Moreover, the same lack of response was observed towards milimolar quantities of benzene, toluene, DMF, NaCl, HCl and NaOH.
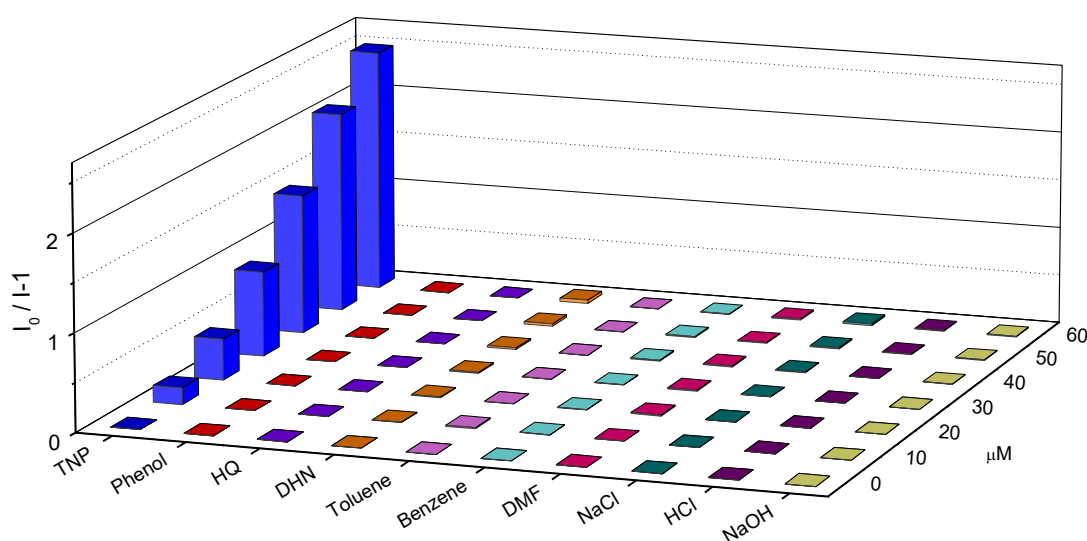

Figure 8. Fluorescence quenching efficiencies of TNF and several commonly found interferents measured on **Pa** thin films immersed in water.

Clearly, other factors affecting the fluorescence quenching of the sensing layer exceed electronic phenomena like the electron-donor and electron-acceptor abilities of the fluorophores/quencher pairs, probably its morphology, the electrostatic interaction with the analyte or the mobility of the excited states within the polymeric matrix. Thus, the quenching responses of the model compounds against TNP and TNT were higher than those observed in the corresponding polymers, $Q_{50\%,\mathbf{P}}/Q_{50\%,\mathbf{M}} \sim 3\text{-}4$ (Fig. 7b). Noteworthy, **Ma** and **Mb** show good response and comparable sensitivity towards TNT, indeed, their response were highly linear and of similar magnitude; and the quenching concentrations needed to reach $Q_{50\%}$ were one order of magnitude lower than those of the polymers.

On the other hand, the general trend in $Q_{50\%}$ was not modified when MeOH was used instead of water in the quenching experiments of **Pa** and **Pb** with TNP and TNT. Actually, upon solvent change to MeOH quenching efficiencies for **Pa** and **Pb** against TNP were high and quite similar to those recorded in water while their already poor efficiencies against TNT decrease ~70% for **Pa** and increased ~70% for **Pb**. These observations suggest that the solvent does not play a substantial role in modifying the quenching ability of polymers **Pa** and **Pb** and that the dynamic interaction between three partners, i. e., solvent, analyte and sensing material, could in this case be reduced to binary analyte-polymer interactions. The nature and extent of molecular interactions between two compounds can be evaluated using the semi-empirical Hansen solubility

parameters (HSPs) [53]. Thus, the solubility parameter distance, R_a, indicates the closeness in cohesive energy densities, *ced*, between sensing material and NACs, $R_a = [4(\delta_{d,sm} - \delta_{d,NAC})^2 + (\delta_{p,sm} - \delta_{p,NAC})^2 + (\delta_{hb,sm} - \delta_{hb,NAC})^2]^{1/2}$, where the cohesive energy densities are expressed as the square of the total solubility parameter, $ced = \delta_t^2 = \delta_d^2 + \delta_p^2 + \delta_{hd}^2$, which is the sum of squares of the partial HSP for the atomic dispersive interactions, δ_d, permanent dipole molecular interactions, δ_p, and hydrogen-bonding interactions, δ_{hb}. Therefore, small R_a indicates high compatibility, that is, the closer the HSP of two interacting species are, the bigger the interaction. Hence, the HSPs of the model compounds and polymers were first calculated using the Stefanis–Panayiotou group-contribution method [54,55] and then the analyte-sensing material distances R_a were evaluated for TNP and TNT.

Table 3. Hansen solubility parameters, HSPs, and solubility arameter distances, *Ra*.

	HSPs				$Ra^{a)}$ vs TNP	$Ra^{a)}$ vs TNT
	δ_d	δ_p	δ_{hb}	δ_t		
Ma	21.4	2.4	5.9	22.3	19.4	16.9
Mb	21.5	5.3	5.0	22.7	17.0	14.0
Pa	22.9	7.3	3.0	24.2	16.4	12.3
Pb	22.9	9.9	3.0	25.1	14.4	9.9

a) Calculated using the HSPs for TNP y TNT from ref. 28.

Interestingly, *Ra* values shown in Table 3 indicate that affinity of the sensing materials with hydrophilic TNP increase in the order **Ma** < **Mb** < **Pa** < **Pb**, however, the quenching efficiency of TNP, evaluated by their $Q_{50\%}$ values, increase in the opposite sense, **Ma** > **Mb** > **Pa** > **Pb**. The same trend was observed with the *Ra* and $Q_{50\%}$ in the case of the hydrophobic TNT. We have reported similar observations regarding two segmented conjugated polymers, one bearing non-polar aliphatic side chains and another with polar oxyethylene side chains [28]. It is relevant at this point to stress again the fast, complete (> 90%) and reversible nature of the quenching process (see Fig. 5). These observations indicate that equilibrium between the concentrations in solution and inside the sensing layer is reached rapidly between successive additions of the quencher. It was also inferred that the mobility of the excited species was comparable in these DSB compounds (Table 1). So, it seems that the kinetic effects due to analyte diffusion inside the film or excited states toward the quencher cannot to be held responsible for the observed trend in quenching efficiencies. The interplay of molecular affinity and morphology could be determining the quenching efficiencies. Although it is not yet clear which are indeed the factors determining that the sensing material turns out to be more sensitive when the affinity with the analytes is lower, this observation could be turned into a useful criteria that could help in the designing of fluorescent sensors along with others like electron donor capacity, amorphous morphology or microporosity.

4. Conclusions

The Wittig-Horner reaction was employed to synthesize new segmented conjugated polymers showing good molecular weights, structural regularity and solution processability despite the absence of solubilizing side chains. The same synthetic route was used to obtain their corresponding model compounds. The morphological studies based on DSC and POM analysis of bulk samples of the model compound and polymers were complemented with the results acquired using spectroscopic methods on thin films. They showed that the amorphous matrix in the thin films contained varying amounts of H- and J-type aggregates whose appearance depend on the thermal history, aging and solvation. Thus, pristine thin films of **Ma** and **Pa** showed closely related spectral features. But the EtO-substitution enhanced the interchromophoric electronic interactions in **Mb** that could only be overcome in **Pb** by the contorted polymeric main chain. The tendency of DSB moieties to form aggregates in the model compounds and the fluctuating behavior of the emission band in **Mb** on the casting conditions, thermal history and solvation is greatly diminished by the polymeric

architecture. The isotropic disposition of chromophores in polymer films is stabilized to such an extent that thermal annealing has no effect in increasing the overall order. Pristine, annealed or hydrated thin films of **Pa** showed similar optical features and the same behavior was seen for and pristine or hydrated films of **Pb**.

Fluorescence quenching by nitroaromatic analytes was fast and reversible pointing to a rapid and easy diffusion of analytes into the DSB-based polymer films. The quenching response to nitrophenols was superior to that against nitrotoluenes. **Pa** and **Ma** showed higher overall quenching efficiencies than **Pb** and **Mb** despite the fact that **Pb** and **Mb** have better electron-donating capabilities. Therefore, the EtO substitution was detrimental to the amorphous morphology and it did not increase sensitivity to NACs. Though it was not anticipated, the sensing abilities of model compounds were higher than those displayed by their parent polymers, however, their thin films are mechanically stable only in plain water, while the casting of transparent thin films and control of the amount of aggregates was much more difficult than in the case of the corresponding polymers. Quenching efficiencies of **Pa** and **Pb** were not modified when MeOH was used instead of water. Thus, in this case the solvent does not play a substantial role in modifying the quenching ability. Moreover, phenol and diphenols as well as commonly found interferents showed negligible effects on the fluorescence emission of **Pa**. Finally, the molecular interactions between analytes and sensing materials were evaluated by their solubility parameter distances, R_a. Interestingly, Ra values indicate that the sensing materials show higher responses when their affinity with the analytes is lower. This observation could be used in the designing of fluorescent sensors along with others more like electron donor capacity, amorphous morphology or material microporosity.

4. References

[1] S. Rochat, T.M. Swager, Conjugated amplifying polymers for optical sensing applications, ACS Appl. Mater. Interfaces 5 (2013) 4488–4502.
[2] Y. Liu, K. Ogawa, K.S. Schanze, Conjugated polyelectrolytes as fluorescent sensors, J. Photochem. Photobiol. C: Photochem. Rev. 10 (2009) 173–190.
[3] M.R. Islam, Z. Lu, X. Li, A.K. Sarker, L. Hu, P. Choi, X. Li, N. Hakobyan, M.J. Serpe, Responsive polymers for analytical applications: A review, Anal. Chim. Acta 789 (2013) 17–32.
[4] C. Li, M. Liu, N. G. Pschirer, M. Baumgarten, K. Müllen, Polyphenylene-based materials for organic photovoltaics, Chem. Rev. 110 (2010) 6817-6855.
[5] A.C. Grimsdale, K. Leok Chan, R.E., Martin, P.G. Jokisz, A.B. Holmes, Synthesis of light-emitting conjugated polymers for applications in electroluminescent devices, Chem. Rev. 109 (2009) 897–1091.
[6] M.C. Scharber, N.S. Sariciftci, Efficiency of bulk-heterojunction organic solar cells, Prog. Polym. Sci. 38 (2013) 1929–1940.
[7] X. Guo, M. Baumgarten, K. Müllen, Designing π-conjugated polymers for organic electronics, Prog. Polym. Sci. 38 (2013) 1832–1908.
[8] V. Strehmel, A.M. Sarker, P.M. Lahti, F.E. Karasz, M. Heydenreich, H. Wetzel, S. Haebel, B. Strehmel, One-and two-photon photochemistry and photophysics of poly(arylenevinylene)s containing a biphenyl moiety, ChemPhysChem. 6 (2005) 267–276.
[9] J. Pina, J. Seixas de Melo, H.D. Burrows, A. L. Maçanita, F. Galbrecht, T. Bunnagel, U. Scherf, Alternating binaphthyl-thiophene copolymers: synthesis, spectroscopy, and photophysics and their relevance to the question of energy migration versus conformational relaxation, Macromolecules, 42 (2009) 1710–1719.
[10] Y. Morisaki, Y. Chujo, Novel [2.2]paracyclophane-fluorene-based conjugated copolymers: synthesis, optical, and electrochemical properties, Macromolecules 37 (2004) 4099–4103.
[11] J.E. Copenhafer, R.W. Walters, T.Y. Meyer, Synthesis and characterization of repeating sequence copolymers of fluorene and methylene monomers, Macromolecules 41 (2008) 31–35.

[12] C.A. Sierra, P.M. Lahti, A photoluminescent, segmented oligo-polyphenylenevinylene copolymer with hydrogen-bonding pendant chains, Chem. Mater. 16 (2004) 55–61.

[13] M.T. Hargadon, E.A. Davey, T.B. McIntyre, D. Gnanamgari, C.M. Wynne, R.C.Swift, J.R. Zimbalist, B.L. Fredericks, A.J. Nicastro, F.E. Goodson, Alternating block copolymers consisting of oligo (phenylene) and oligo (ethylene glycol) units of defined length: Synthesis, thermal characterization, and light-emitting properties, Macromolecules 41 (2008) 741–750.

[14] S.V. Chasteen, S.A. Carter, G. Rumbles, The effect of broken conjugation on the excited state: Ether linkage in the cyano-substituted poly (p-phenylene vinylene) conjugated polymer poly (2,5,2′,5′-tetrahexyloxy-8,7′-dicyano-di-p-phenylene vinylene), J. Chem. Phys. 124 (2006) 214704.

[15] H.C. Yeh, C.H. Chien, P.I. Shih, M.C. Yuan, C.F. Shu, Polymers derived from 3,6-fluorene and tetraphenylsilane derivatives: solution-processable host materials for green phosphorescent OLEDs. Macromolecules, 41 (2008) 3801–3807.

[16] G. Singh, A. Hamid, R.M. Peetz, Studies on homologous random and alternating segmented conjugated polymers with and without silicon synthesized by ADMET, Polym. Chem. 7 (2016) 669–679.

[17] J. Osio Barcina, M.R. Colorado Heras, M. Mba, R. Gomez Aspe, N. Herrero-Garcia, Efficient electron delocalization mediated by aromatic homoconjugation in 7,7-diphenylnorbornane derivatives, J. Org. Chem. 74 (2009) 7148–56.

[18] R. Fáber, A. Staško, O. Nuyken, New polymers based on fluorenylidene-linked conjugated oligo(p-phenylene)s, Macromol. Chem. Phys. 202 (2001) 2321–2327.

[19] M. Beinhoff, L.D. Bozano, J.C. Scott, K.R. Carter, Design and synthesis of new polymeric materials for organic nonvolatile electrical bistable storage devices: poly(biphenylmethylene)s, Macromolecules 38 (2005) 4147–4156.

[20] P.G. Del Rosso, M.F. Almassio, S.S. Antollini, R.O. Garay, Optical characterization of amorphous oligo(4,4´-biphenylene-1,1-substituted methylene)s, Opt. Mater. 30 (2007) 478–485.

[21] P.G. Del Rosso, M.F. Almassio, P. Aramendia, S.S. Antollini, R.O. Garay, Poly[(2,2,5,2-tetramethoxy-p-terphenyl-5,5-ylene)propylene]: Synthesis and physical properties of a novel amorphous regularly segmented conjugated polymer, European Polym. J. 43 (2007) 2584–2593.

[22] J.K. Herrema, J. Wildeman, R.E. Gill, R.H. Wieringa, P.F. van Hutten, G. Hadziioannou, Tuning of the luminescence in multiblock alternating copolymers. 1. Synthesis and Spectroscopy of Poly[(silanylene)thiophene]s. Macromolecules 28 (1995) 8102–8116.

[23] A.M. Sarker, B. Strehmel, D.C. Neckers, Synthesis, characterization, and optical properties of copolymers containing fluorine-substituted distyrylbenzene and nonconjugated spacers. Macromolecules 32 (1999) 7409–7413.

[24] C. Xia, R.C. Advincula, Ladder-type oligo (p-phenylene) s tethered to a poly (alkylene) main chain: the orthogonal approach to functional light-emitting polymers, Macromolecules 34 (2001) 6922–6928.

[25] P.G. Del Rosso, M.F. Almassio, R.O. Garay, Chemosensing of nitroaromatics with a new segmented conjugated quaterphenylene polymer, Tetrahedron Lett. 52 (2011) 4911–4915.

[26] P.G. Del Rosso, M.F. Almassio, G.R. Palomar, R.O. Garay, Nitroaromatic compounds sensing. Synthesis, photophysical characterization and fluorescence quenching of a new amorphous segmented conjugated polymer with diphenylfluorene chromofores, Sens. Actuators B: Chem. 160 (2011) 524–532.

[27] S.B. Jagtap, D.D. Potphode, T.K. Ghorpade, A.K. Palai, M. Patri, S.P. Mishra, t-Butyl pyrene containing poly (arylene ethynylene) s for highly sensitive and selective sensing of TNT, Polymer 55 (2014) 2792-2798.

[28] P.G. Del Rosso, M.J. Romagnolli, M.F. Almassio, C.A. Barbero, R.O. Garay, Diphenylanthrylene and diphenylfluorene-based segmented conjugated polymer films as fluorescent chemosensors for nitroaromatics in aqueous solution, Sensors and Actuators B: Chemistry 203 (2014) 612–620.

[29] J. Gierschner, S. Y. Park, "Luminescent distyrylbenzenes: tailoring molecular structure and crystalline morphology." J. Mater. Chem. C 1 (2013) 5818–5832.

[30] R.E. Di Paolo, H.D. Burrows, J. Morgado, A.L. Maçanita, Photodynamics of a PV trimer in high-viscosity solvents and in pmma films: a new insight into energy transfer versus conformational relaxation in conjugated polymers, ChemPhysChem, 10 (2009) 448–454.

[31] S.H. Lim, T.G. Bjorklund, C.J. Bardeen, Characterization of individual submicron distyrylbenzene aggregates using temperature-dependent picosecond fluorescence and atomic force microscopy, J. Phys. Chem. B 108 (2004) 4289–4295.

[32] E.M. Kyllo, T.L. Gustafson, D. K. Wang, R.G. Sun, A. J. Epstein, Photophysics of segmented block PPV copolymer derivatives, Synth. Met. 116 (2001) 189–192.

[33] B. Ali, S. Jabar, W. Salih, R.K. Al Tamimi, H. Al Attar, A.P. Monkman, Synthesis and spectroscopic characterization studies of low molecular weight light emitting PPV segmented copolymers, Opt. Mater. 32 (2009) 350–357.

[34] O.D. Bernardinelli, S.M. Cassemiro, L.A.D.O. Nunes, T.D.Z. Atvars, L. Akcelrud, E.R. deAzevedo, Correlations between conjugation length, macromolecular dynamics, and photophysics of phenylene-vinylene/aliphatic multiblock copolymers, The Journal of Physical Chemistry B 116 (2012) 5993–6002.

[35] J. Neuwoehner, A. Schofer, B. Erlenkaemper, K. Steinbach, K. Hund-Rinke, A. Eisentraeger,. Toxicological characterization of 2, 4, 6-trinitrotoluene, its transformation products, and t o nitramine explosives, Environ. Toxicol. Chem. 26 (2007) 1090–1099.

[36] M.A. Rubio, E. Lissi, N. Herrera, V. Pérez, N. Fuentes, Phenol and nitrophenols in the air and dew waters of Santiago de Chile, Chemosphere 86 (2012) 1035–1039.

[37] F Neese, The ORCA program system, Wiley Interdiscip. Rev.: Comput. Mol. Sci. 2 (2012) 73−78.

[38] A.R. Allouche, Gabedit - A graphical user interface for computational chemistry softwares, J. Comp. Chem. 32 (2011) 174−182.

[39] Sure R, Grimme S. Corrected Small Basis Set Hartree-Fock Method for Large Systems. J Comput Chem. 34 (2013) 1672–1685.

[40] Grimme S, Ehrlich S, Goerigk L. Effect of the Damping Function in Dispersion Corrected Density Functional Theory. J Comput Chem. 32 (2011) 1456–1465.

[41] Grimme S, Antony J, Ehrlich S, Krieg H. A consistent and accurate ab initio parametrization of density functional dispersion correction (DFT-D) for the 94 elements H-Pu. J Chem Phys. 132 (2010) 154104.

[42] Kruse H, Grimme S. A geometrical correction for the inter- and intra-molecular basis set superposition error in Hartree-Fock and density functional theory calculations for large systems. J Chem Phys. 136 (2012) 154101.

[43] J.H. Wood, R.E. Gibson, Di-(α-and β-substituted aminoethyl)-benzenes. I. 2, 5-bis-(2-aminoethyl)-hydroquinones, J. Am. Chem. Soc. 71 (1949) 393−395.

[44] N. Benfaremo, D.J. Sandman, S. Tripathy, J. Kumar, K. Yang, M.F. Rubner, C. Lyons, Synthesis and characterization of luminescent polymers of distyrylbenzenes with oligo(ethylene glycol) spacers, Macromolecules 31 (1998) 3595−3599.

[45] M.J. Plater, T. Jackson, Polyaromatic amines. Part 3: Synthesis of poly (diarylamino) styrenes and related compounds, Tetrahedron 59 (2003) 4673−4685.

[46] N.N. Barashkov, D.J. Guerrero, H.J. Olivos, J.P. Ferraris, Synthesis and optical properties of oligo-and poly (2,5-dialkoxy-1,4-para-phenylenevinylene)s, Synth. Met. 75(1995) 153−160.

[47] J. Gierschner, M. Ehni, H.J. Egelhaaf, B.M. Medina, D. Beljonne, H. Benmansour, G.C. Bazan, Solid-state optical properties of linear polyconjugated molecules: π-stack contra herringbone, J. Chem. Phys. 123 (2005) 144914.

[48] K.-H. Schweikhart, M. Hohloch, E. Steinhuber, M. Hanack, L. Lüer, J. Gierschner, H.-J. Egelhaaf, D. Oelkrug, Highly luminescent oligo (phenylenevinylene) films: the stereochemical approach, Synth. Met. 121 (2001) 1641−1642.

[49] F. Bencheikh, D. Duché, C.M. Ruiz, J.J. Simon, L. Escoubas, Study of Optical Properties and Molecular Aggregation of Conjugated Low Band Gap Copolymers: PTB7 and PTB7-Th, J. Phys. Chem. C. 119 (2015) 24643-24648.

[50] S. Shanmugaraju, P.S. Mukherjee, π-Electron rich small molecule sensors for the recognition of nitroaromatics, Chem. Commun. 51(2015) 16014-16032.

[51] J.C. Sanchez, S.A. Urbas, S.J. Toal, A.G. DiPasquale, A.L. Rheingold, W.C. Trogler, Catalytic hydrosilylation routes to divinylbenzene bridged silole and silafluorene polymers. Applications to surface imaging of explosive particulates, Macromolecules 41 (2008) 1237-1245.

[52] G. He, N. Yan, J. Yang, H. Wang, L. Ding, S. Yin, Y. Fang, Pyrene-containing conjugated polymer-based fluorescent films for highly sensitive and selective sensing of TNT in aqueous medium, Macromolecules 44 (2011) 4759-4766.

[53] C. M. Hansen, Hansen Solubility Parameters: A Users Handbook, 2nd Ed., CRC Press LLC, Boca Raton, FL, 2007.

[54] E. Stefanis, C. Panayiotou, Prediction of Hansen solubility parameters with a new group-contribution method, Int. J. Thermophys. 29 (2008) 568–585.

[55] E. Stefanis, C. Panayiotou, A new expanded solubility parameter approach, Int. J. Pharm. 426 (2012) 29–43.